THE ASTROPHYSICAL JOURNAL, 426:334–339, 1994 May 1

MODELING AND INTERPRETATION OF THE OPTICAL AND *HST* UV SPECTRUM OF SN 1993J

E. BARON,[1] P. H. HAUSCHILDT,[2] AND D. BRANCH[1]
Received 1993 September 24; accepted 1993 November 5

ABSTRACT

We present spherically symmetric, non–LTE, expanding model atmosphere synthetic spectra of SN 1993J and compare them to the ultraviolet and optical spectra obtained simultaneously on 1993 April 15 by the *HST* and at Lick Observatory. We are able to fit the optical and *HST* near-UV spectra with a variety of compositions, but find that our best fits are obtained with an enhanced helium abundance ($Y = 0.8$) and significant nonthermal ionization due to gamma rays produced by the decay of ^{56}Ni. We find the effects of X-rays produced by thermal bremsstrahlung in the circumstellar material to have little effect on the spectrum. Our current models are unable to fit the *HST* far-UV region, predicting too little flux and strong, unseen Fe II features.

Subject headings: radiation mechanisms: nonthermal — supernovae: individual (SN 1993J) — ultraviolet: stars

1. INTRODUCTION

Supernova SN 1993J in the nearby galaxy M81 has been classified as a peculiar Type II supernova. Early spectra (for a review see Wheeler & Filippenko 1994) showed strong hydrogen Balmer lines, but after April 22 there was a transition of the Hα line to a "double-peaked" structure (Hu et al. 1993) which has been recognized as the emergence of the He I λ6678 line (Filippenko & Matheson 1993; Filippenko, Matheson, & Ho 1993). The light curve also shows a peculiar structure, declining very rapidly in all bands until about April 6 and then reaching a secondary maximum near April 18.

Based on the behavior of the light curve and the appearance of strong helium lines in the later spectra, several authors have suggested that the progenitor was a member of a close binary system, having lost all but a few tenths of a solar mass of its hydrogen envelope to the companion (Bartunov et al. 1994; Filippenko & Matheson 1993; Filippenko et al. 1993; Nomoto et al. 1993; Podsiadlowski et al. 1993; Schmidt et al. 1993; Swartz et al. 1993; Woosley et al. 1993b; Woosley, Eastman, & Weaver 1993a). For an alternative view see Höflich, Langer, & Duschinger (1993).

This class of supernova, for which SN 1987K is the archetype, has been referred to as Type IIb (Woosley, Pinto, & Ensman 1988) in comparison to Type Ib, which are thought to be physically similar systems except that in the SN Type Ib case the entire hydrogen envelope has been stripped away.

In this paper we present our initial analysis of the combined UV and optical spectrum obtained by the *HST* and at Lick Observatory (Jeffery et al. 1993).

2. MODELS

2.1. *Model Construction*

In order to extract detailed quantitative information on velocities, densities, temperatures, and compositions, and to constrain theoretical explosion models, it is necessary to analyze the supernova spectrum in detail, via synthetic spectral modeling. We use the computer code PHOENIX 4.2 to compute our model atmospheres and synthetic spectra for SN 1993J. This is an updated version of the code used for the analyses of the early spectra of Nova Cygni 1992 (Hauschildt et al. 1994); therefore we give here only a short description.

PHOENIX uses an accelerated Λ-iteration (ALI or operator splitting) method to solve the time-independent, spherically symmetric, *fully* relativistic radiative transfer equation for lines and continua, to all orders in v/c including the effects of relativistic Doppler shift, advection, and aberration (Hauschildt 1992a). The multilevel, non–LTE rate equations are solved self-consistently for H I, He I, He II, Mg II, Ca II, and Na I, using an ALI method (Rybicki & Hummer 1991; Hauschildt 1993; Baron & Hauschildt 1993). Simultaneously we solve for the special relativistic condition of radiative equilibrium in the Lagrangian frame (Hauschildt 1992b) using either a partial linearization or a modified Unsöld-Lucy temperature correction scheme. The relativistic effects, in particular the first-order effects of advection and aberration, are important at the high expansion velocities observed in typical SNs (Hauschildt, Best, & Wehrse 1991). We have obtained good convergence for the models presented in this paper.

The generalized (for non–LTE) equation of state (EOS) is solved for 40 elements and up to six ionization stages per element, for a total of 176 species. Test calculations showed that, for the conditions found in SNs at the stage of their spectral evolution we consider here, molecules and negative ions are unimportant and we neglect them with the benefit of substantial savings in CPU time. The numerical solution of the EOS is based on Brent's method for the solution of nonlinear equations (Brent 1973) which is very robust and fast.

In addition to the non–LTE lines, the models include, self-consistently, line blanketing of the most important ($\approx 10^5$) metal lines selected from the latest atomic and ionic line list of Kurucz (1993). The entire list contains close to 42 million lines, but not all of them are important for the case at hand. Therefore, before every temperature iteration, a smaller list is formed from the original list. First an optical depth point is chosen, usually at $\tau_{\rm std} \approx 0.01$. Then, using the density and temperature for this depth, the absorption coefficient in the line center, κ_l, is calculated for every line and compared to the corresponding continuum (LTE + non–LTE) absorption coefficient, κ_c. A

[1] Department of Physics and Astronomy, University of Oklahoma, 440 West Brooks, Room 131, Norman, OK 73019-0225.
[2] Department of Physics and Astronomy, Arizona State University, Tempe, AZ 85287-1504.

line is transferred to the "small list" if the ratio κ_l/κ_c is larger than a prespecified value (usually 10^{-4}). In the subsequent radiative transfer calculations all lines selected in this way are taken into account as individual lines, and all others from the large line list are neglected. This selection procedure is repeated at *every* iteration in order to always include the most important lines. We treat line scattering in the metal lines by parameterizing the albedo for single scattering, α. The calculation of α would require a full non–LTE treatment of *all* lines and continua, which is outside the scope of this paper. Tests have shown that as a direct result of the velocity gradient in nova photospheres, the shape of the lines does not depend sensitively on α and our approach is a reasonable first approximation. Therefore, we adopt an average value of $\alpha = 0.95$ for all metal lines. The continuous absorption and scattering coefficients are calculated using the cross sections as described in Hauschildt et al. (1992).

We treat the effects of impinging radiation by assuming that the outer boundary condition for the incoming radiation field is isotropic and has the spectral form of thermal bremsstrahlung with a radiation temperature specified by $T_{\rm circ}$ (which we take to be in the range 10^8–10^9 K) and a total luminosity of $L_x = 5 \times 10^{39}$ ergs s^{-1} (Tanaka 1993). The impinging radiation field is used as the outer boundary condition for the relativistic radiative transfer; thus we are able to compute the penetration depth for the radiation consistently. The resulting radiation field is also used for the solution of the multilevel non–LTE transfer problem and results in nonthermal radiative excitation and ionization of the non–LTE species.

The effects of nonthermal collisional ionization by primary electrons produced by collisions with gamma rays due to the decay of ^{56}Ni are modeled using the continuous slowing-down approximation (Garvey & Green 1976; Swartz 1991). We neglect the effect of secondary electrons, since most of their energy is thermalized and thus does not affect the level populations directly (Meyerott 1980). The collisional cross sections are taken from the work of Lotz (1967a, b; 1968a, b, c) and the ions included are H I, He I, He II, and Na I. We neglect the nonthermal ionization of Mg II and Ca II because we are lacking some of the relevant atomic data for those ions.

2.2. *The Model Parameters*

The model atmospheres are characterized by the following parameters (see Hauschildt et al. 1992 for details): (i) the reference radius R_0, which is the radius where the continuum optical depth in extinction at 5000 Å is unity; (ii) the effective temperature $T_{\rm eff}$, which is defined by means of the luminosity, L, and the reference radius, R_0, [$T_{\rm eff} = (L/4\pi R_0^2\,\sigma)^{1/4}$, where σ is Stefan's constant]; (iii) the density structure parameter, v_e, [$\rho(r) \propto \exp(-v/v_e)$]; (iv) the expansion velocity, v_0, at the reference radius; (v) the density, $\rho_{\rm out}$, at the outer edge of the envelope; (vi) the metal-line threshold ratio, Γ, (vii) the albedo for line scattering (metal lines only, here set to 0.95); (viii) the statistical velocity ξ, treated as depth-independent isotropic turbulence, and (ix) the element abundances. The influence of the nonthermal radiative and collisional excitation and ionization is discussed in detail in the subsequent sections.

We emphasize that for extended model atmospheres one should not assign, a priori, a physical interpretation to the parameter combination of $T_{\rm eff}$ and R_0. While $T_{\rm eff}$ has a well-defined physical meaning for plane-parallel stellar atmospheres, its definition for extended atmospheres is connected to the particular definition of the radius R_0 (see Buschek, Scholz, & Wehrse 1991). In addition, the reference radius R_0 in our models is defined using a *continuum* optical depth scale at $\lambda = 5000$ Å and is not directly comparable to observationally derived radii. Therefore, the effective temperature is not well-defined for extended atmospheres and must be regarded only as a convenient numerical parameter.

We take the explosion date to be March 27–28 and assume that the extinction to the supernova is given by $E(B-V) = 0.1$ mag (Baron et al. 1993; Jeffery et al. 1993; Wheeler & Filippenko 1994). In these calculations Mg II and He II are treated in LTE.

3. RESULTS

3.1. *Solar Abundance Models*

We first turn our attention to models with solar abundances. Figure 1 displays a fit (model Sol1) to the observed UV and optical spectrum. In this paper the models are compared to the data calibrated exactly as presented by Jeffery et al. (1993). In model Sol1, the effective temperature is $T_{\rm eff} = 6500$ K. Although the calculations are not directly comparable our $T_{\rm eff}$ is a bit higher than the 6000 K found by Jeffery et al. (1993), while our reference velocity $v_0 = 8500$ is similar to their value of 8000 km s^{-1}. The model parameters are listed in Table 1.

In this calculation we have ignored all effects due to either the decay of ^{56}Ni or to X-rays produced by circumstellar interaction. The model appears to be too bright in the blue (3000–5000 Å) and too faint in the UV (2000–3000 Å). In all of the models we have calculated, the flux in the UV is a factor of 5–10 too small, and, in agreement with Jeffery et al. (1993), our

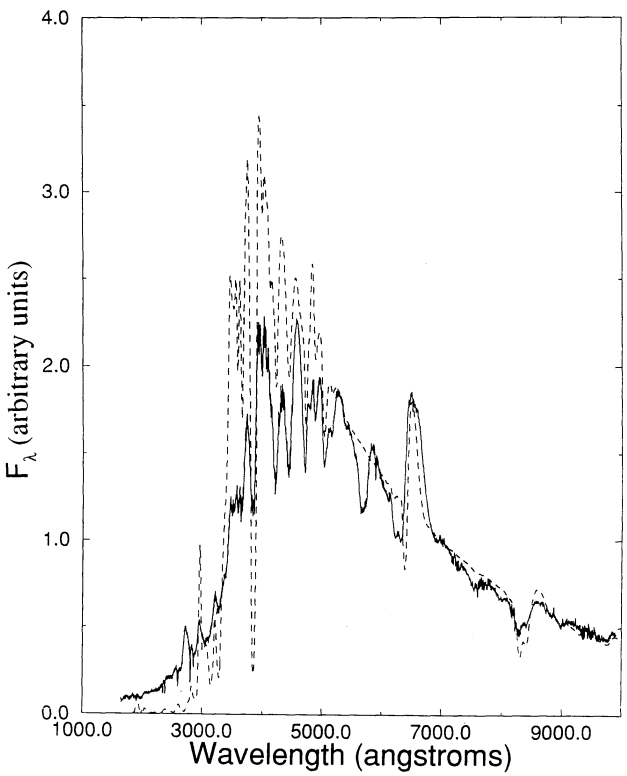

FIG. 1.—A synthetic spectrum (Model Sol1, *dashed line*) is compared to the combined spectrum obtained by the *HST* and at Lick Observatory (*solid line*) of SN 1993J on April 15. The model effective temperature is $T_{\rm eff} = 6500$ K, and the other model parameters are listed in Table 1.

TABLE 1

PARAMETERS OF THE MODELS[a]

Model	[He]	$T_{\rm eff}$	R_0 (10^{15} cm)	v_0 (km s^{-1})	v_e (km s^{-1})	$X_{\rm Ni}$	$T_{\rm circ}$
Sol1	0.00	6500	1.3	8500	450		
Sol1*n*th	0.00	6500	1.3	8500	450	0.1	
Sol2	0.00	6500	1.4	9000	600		
Sol3	0.00	5900	1.4	9000	600		
He1	1.01	5900	1.4	9000	600		
He1*n*th	1.01	5500	1.4	9000	600	0.1	
He2*n*th	1.01	5900	1.4	9000	600	0.01	
He3*n*th	1.01	5900	1.4	9000	600	0.03	
He2*n*thX	1.01	5900	1.4	9000	600	0.01	10^8
He3*n*thX	1.01	5900	1.4	9000	600	0.03	10^9
HeCo1*n*th ...	1.01	6500	1.4	9000	600	0.05	

[a] NOTE.—[He] is the logarithm of the ratio of the helium abundance to the solar helium abundance (by number), $T_{\rm eff}$, R_0, v_0 are the "effective" temperature, radius, and velocity at the reference point $\tau_{\rm std} = 1$, v_e is the parameter that characterizes the density profile, $X_{\rm Ni}$ is a parameter that specifies the mass fraction of nickel to take into account the effects of nonthermal ionization, and $T_{\rm circ}$ parameterizes the spectrum of impinging X-ray radiation.

calculations predict strong Fe II absorption features whereas the observed spectrum is nearly featureless. While the positions of the weak Fe II absorption lines λ5018 and λ5169 are well reproduced, the Balmer lines appear to be not quite blueshifted enough. While the Ca II infrared triplet is reasonably well fitted, the H + K doublet is far too strong and the absorption of Hα is too strong, the emission is slightly too weak and the equivalent width is too small. In none of our calculations are we able to reproduce the detailed structure of the absorption feature just redward of Hα. The feature at around 5600 Å, which we have previously identified (Baron et al. 1993) as due to either the He I λ5876 line or the Na D doublet, is clearly not fitted in this calculation. Thus it seems unlikely that the feature at 5600 Å is due to a solar composition of sodium.

In model Sol1*n*th we have included the effects due to the decay of ^{56}Ni. We have assumed, for the purposes of calculating the energy input that the nickel is uniformly mixed throughout the atmosphere with a mass fraction $X_{\rm Ni} = 0.1$ and that the nickel was produced as ^{56}Ni, 19 days before the spectrum is calculated. Since in our present calculations the composition is necessarily uniform and we see no evidence of a nickel, cobalt, iron-dominated atmosphere, we have not included such a large mass fraction of nickel in the equation of state, i.e., in the formation of the spectrum. Thus, $X_{\rm Ni}$ serves only as a parameter to determine the amount of nonthermal ionization rather than being the true nickel mass fraction. To this extent, our procedure is not self-consistent. We plan to investigate the effects of higher nickel and cobalt abundances on the model atmospheres and the synthetic spectra in detail in future work. We present one model with a significantly enhanced nickel, cobalt, and iron abundance below.

Even with this large amount of nonthermal collisional ionization, there are not enough helium atoms to provide absorption features in the spectrum. Even though the ionization of helium is very high (the departure coefficients of the ground state are as low as 10^{-21} compared to $\sim 10^{-3}$ in the case of model Sol1), there is not enough optical depth in the line to produce a significant feature in the observed spectrum. Thus we must increase the helium concentration in order to obtain a fit to the spectrum. We examine enhanced helium models in the following subsection.

In models Sol2 and Sol3 we have attempted to improve the quality of the fit using solar abundances. In model Sol2 we have increased the reference velocity to $v_0 = 9000$ km s^{-1} while at the same time making the density profile somewhat less steep by increasing the parameter v_e to 600 km s^{-1}, corresponding to a power-law index at the reference point, $N = 15$, with $\rho \propto R_0^{-N}$. The positions of the absorption features of the weak iron lines remain quite good, and the positions of the absorption features of the Balmer lines are somewhat improved. The model is still too bright in the blue, and the flux continues to be too low in the UV. In model Sol3 (Fig. 2) we have reduced the temperature to $T_{\rm eff} = 5900$ K and the fit in the blue is significantly improved.

3.2. *Enhanced Helium Models*

Figure 3 (model He1) shows a fit to the observed spectrum, neglecting all nonthermal processes and with the helium concentration equal to that of hydrogen by number while keeping the metal to hydrogen ratio constant, thus $Y \sim 0.8$. The model parameters are $T_0 = 5900$ K, $R_0 = 1.4 \times 10^{15}$ cm, $v_0 = 9000$ cm s^{-1}, and $v_e = 600$ cm s^{-1}, so the model is identical to the solar composition model Sol3 except that the helium concentration has been increased by a factor of 10 by number. The fit is quite good and the height and equivalent width of the Hα emission are very close to the observed values, although the absorption remains too strong and the feature blueward of the Hα absorption is not present. The blue is fitted very well, but the flux continues to be too low in the UV. Also any evidence of an He I λ5876 line is lacking, as to be expected at these temperatures. In order to investigate if a strong He I λ5876 line

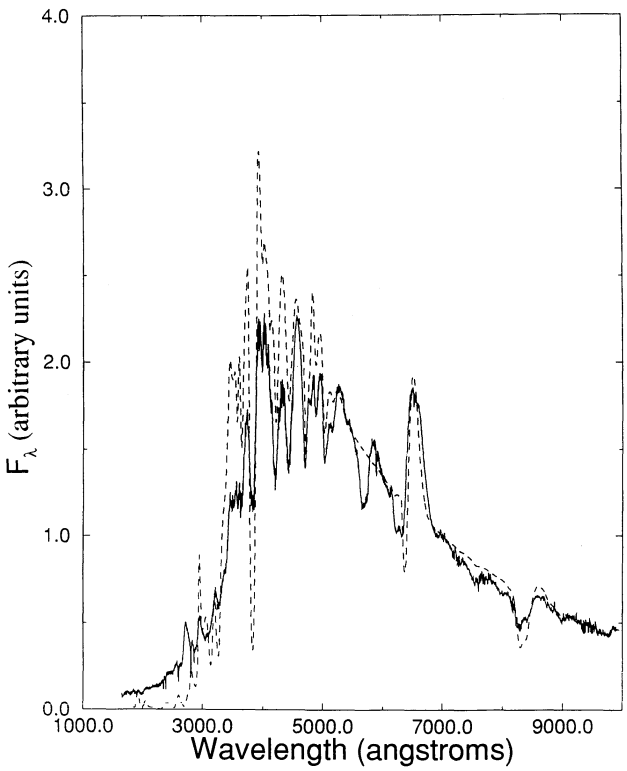

FIG. 2.—A synthetic spectrum (Model Sol3, *dashed line*) is compared to the combined spectrum obtained by the *HST* and at Lick Observatory (*solid line*) of SN 1993J on April 15. The model effective temperature is $T_{\rm eff} = 5900$ K, and the other model parameters are listed in Table 1.

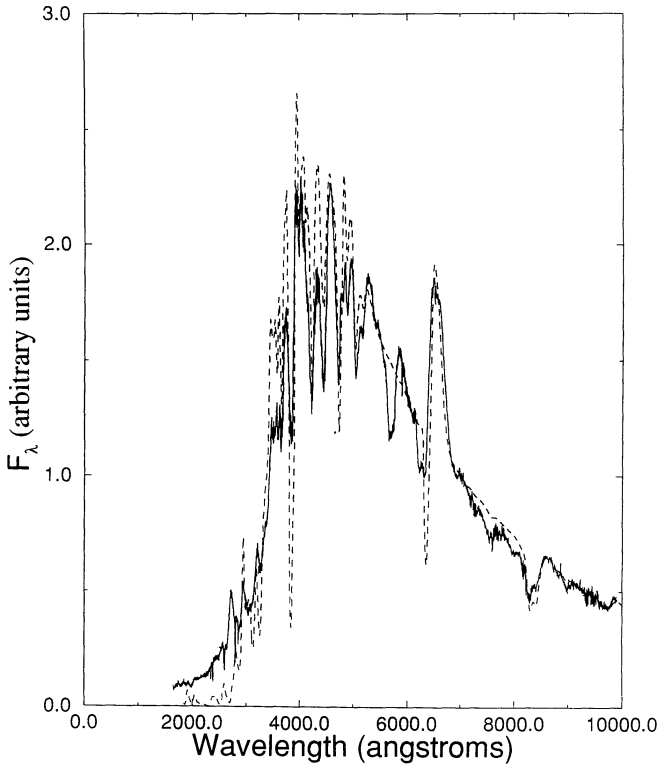

FIG. 3.—A synthetic spectrum (Model He1, *dashed line*) is compared to the combined spectrum obtained by the *HST* and at Lick Observatory (*solid line*) of SN 1993J on April 15. The model effective temperature is $T_{\rm eff} = 5900$ K, and the other model parameters are listed in Table 1.

can be produced by nonthermal collisional ionization, we calculated the model He1*n*th in which we have set the nickel mass fraction to $X_{\rm Ni} = 0.1$. The model parameters are the same as in model He1, with the exception of the inclusion of nonthermal ionization due to ^{56}Ni. In this model, the He I λ5876 absorption is too strong, but the emission is not strong enough. Both the strong lines He I λ5876 and Hα show absorption profiles that are not reproduced in the model calculations. It seems likely that the large absorption widths are produced by some material at high velocity. Since our models have very steep atmospheres, it seems likely that there exists a small amount of material external to the steep atmosphere with a shallower profile. Since it shows up only in the absorption of the strong lines, the total amount of mass in the shallow external region must be very small.

In an attempt to determine the total amount of nickel mixed into the atmosphere we calculated models with $X_{\rm Ni} = 0.01$ (model He2*n*th) and $X_{\rm Ni} = 0.03$ (model He3*n*th). The spectrum for model He3*n*th which represents our best fit to the observed spectrum is displayed in Figure 4. We conclude that the total fraction of nickel required to fit the depth of the He I λ5876 line lies in the range $X_{\rm Ni} = 0.03$–0.10 and is probably closer to 0.03 than to 0.10.

It is clear from both the radio and X-ray observations that SN 1993J interacted with a circumstellar medium. In order to model the effects of the X-rays on the spectrum we chose an outer boundary condition to consist of a thermal bremsstrahlung spectrum parameterized by a temperature $T_{\rm circ}$ with a total luminosity of 5×10^{39} ergs s^{-1} (Tanaka 1993). In model He2*n*thX the parameters are the same as for He2*n*th, but $T_{\rm circ} = 10^8$ K, while in model He3*n*thX the parameters are the same as for He3*n*th, but $T_{\rm circ} = 10^9$ K. In neither case do the impinging X-rays produce a noticeable effect on the calculated spectra. This is in spite of the fact that the departure coefficient of the hydrogen ground state has decreased by a factor of about 1000 near the surface.

3.3. *Enhanced Cobalt Abundance*

Figure 5 presents a calculation where we have increased the atmospheric abundance of nickel, cobalt, and iron to correspond to a nickel fraction of $X_{\rm Ni} = 0.1$ produced 19 days previously. While there is some evidence for Co II lines in the red, the model does a significantly worse job in fitting the near-UV and predicts Fe II features near 5000 Å that are too strong. Reducing the temperature does not significantly reduce the strength of the Fe II features. For LTE Fe II atoms we do not find evidence of enhanced iron in the photosphere.

4. DISCUSSION

Our best fits to the observed spectrum are models Sol3, He1, He2*n*th, and He3*n*th. Thus, we can conclude that the effective temperature is $T_{\rm eff} \approx 5900$ K, the reference velocity $v_0 \approx 9000$ km s^{-1}, the reference radius is (assuming homology) $R_0 \approx 1.4 \times 10^{15}$ cm, and that the *e*-folding velocity is $v_e \approx 600$ km s^{-1}, or that the density exponent at the reference point is $N \approx 15$. It seems clear that fitting the feature at 5600 Å requires a large helium fraction, $Y \approx 0.8$, and a large amount of nickel must be mixed into the atmosphere.

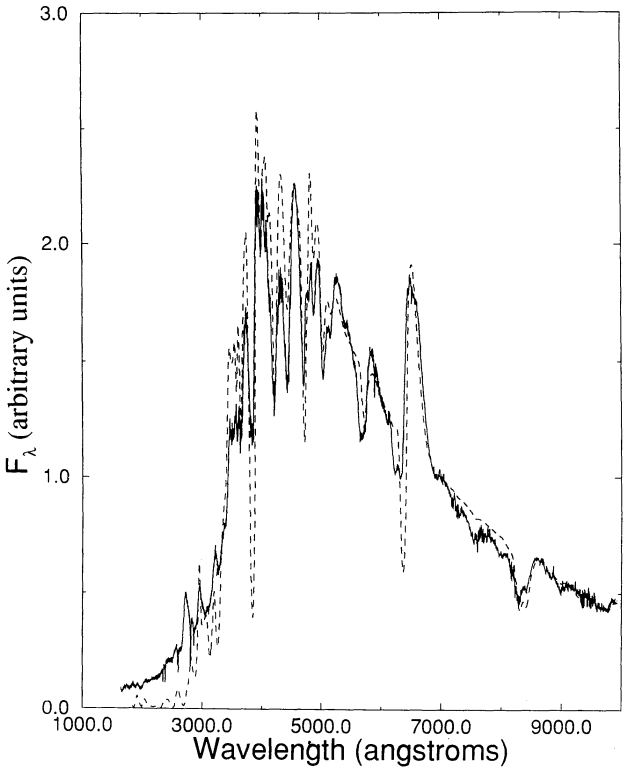

FIG. 4.—A synthetic spectrum (Model He3*n*th, *dashed line*) is compared to the combined spectrum obtained by the *HST* and at Lick Observatory (*solid line*) of SN 1993J on April 15. The model effective temperature is $T_{\rm eff} = 5900$ K, the effects of nonthermal ionization of ^{56}Ni are included ($X_{\rm Ni} = 0.03$), and the other model parameters are listed in Table 1.

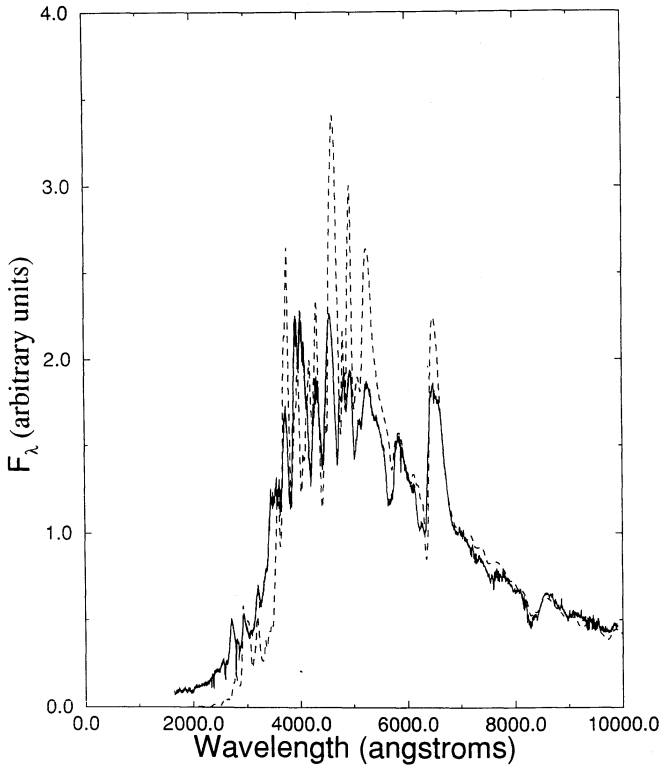

FIG. 5.—A synthetic spectrum (Model HeCo1*n*th, *dashed line*) is compared to the combined spectrum obtained by the *HST* and at Lick Observatory (*solid line*) of SN 1993J on April 15. The model effective temperature is $T_{\rm eff}$ = 6500 K, the effects of nonthermal ionization of ^{56}Ni are included ($X_{\rm Ni} = 0.05$), and the composition has been altered so that the mass fraction of nickel, cobalt, and iron corresponds to the decay products of a mass fraction of nickel of 0.1.

Models of the light curve have been calculated by Shigeyama et al. (1994) who find a good fit to the light curve with a 4 $M_\odot$ helium core, a H/He envelope ($Y = 0.8$) of mass 0.89 $M_\odot$, and a total nickel mass of 0.075 $M_\odot$. Thus, our results are in excellent agreement with the light curve models. Taking as our range of the nickel mass fraction $X_{\rm Ni} = 0.03$–0.10 and assuming uniform mixing throughout the core and a baryon mass of the neutron star of 1.6 $M_\odot$, we would predict for the Shigeyama et al. (1994) model a total nickel mass of 0.10–0.33 $M_\odot$, with the low value being the preferred one. On the other hand, our nickel fraction is likely to be an overestimate both due to the facts that we do not model the gamma-ray transport at all and that we neglect the effect of nonthermal bound-bound interactions as well as secondary electron interactions.

Our models all predict a UV flux that is a factor of 5–10 too low and our UV spectra have Fe II absorption and emission features that are too strong. On the other hand, all of the line blanketing in the UV comes from species that we treat in LTE, so the effects of nonthermal ionization are neglected in that part of the spectral region. The other poorly fitted feature is Ca II H + K, which in all our models is far too strong even though the infrared triplet is reasonably well fitted. This too may be due to our neglect of nonthermal ionization of Ca II. In addition *HST* has trouble with scattered light below ~2300 Å and it may be that the observed spectrum suffers from such contamination.

It is possible that there is additional radiation produced by the circumstellar interaction that could lead to an increased flux in the UV region as well as increased emission in the strong lines such as Hα and Ca II H + K; modeling such effects as well as treating nonthermal ionization of Ca II will be the subject of future work.

5. DISTANCE ESTIMATE

Since our models predict the total emitted flux, we can convolve our flux with standard filters to predict absolute magnitudes for our models. Taking only the best-fit models to the April 15 spectrum Sol3, He1, He2*n*th, and He3*n*th, we find the distance to the supernova to be 3.4 ± 0.1 Mpc which is lower than, but consistent within the errors with, our previous estimate of 4.0 ± 0.5 Mpc (Baron et al. 1993). Convolving all of our synthetic fits to the spectra taken on April 7, 13, and 15, we find a distance to the supernova of 3.9 ± 0.6 Mpc which is consistent with the recent Cepheid distance 3.6 ± 0.3 Mpc (Freeman et al. 1993).

Schmidt et al. (1993), using a different version of the expanding photosphere method, find a distance to SN 1993J of 2.6 Mpc. They find the photospheric velocity on April 13 to be 7900 km s^{-1} based on the positions of the lines Fe II λ5018, λ5169. They have suggested (B. P. Schmidt 1993, private communication; Wheeler & Filippenko 1994) that the source of the discrepancy in the distance measurement is due solely to our higher velocities. Part of this confusion is the result of our loosely, and incorrectly, referring to our reference point $\tau_{\rm std} = 1$ as the "photosphere." Neither in these calculations nor in our previous paper (despite a somewhat misleading statement in that paper) have we determined the value of v_0 by measuring the velocity of a single line or set of lines. The parameters are determined by the quality of the fit to the complete spectrum, which we believe to be the only correct way to overcome compensations in the parameters which may occur when one looks at only a few selected lines (Best & Wehrse 1993). In these models the concept of a gray photosphere is not applicable and one should refer to the line-forming region. In extended atmospheres the line-forming region is expected to be in the neighborhood of our reference radius, but can occur at higher or lower velocities depending on the strength of the line one is considering, as well as the neighboring continuum and radiative transfer effects. Comparing the positions of the absorption features in model Sol1 (v_0 = 8500 km s^{-1}) to those in model Sol2 (v_0 = 9000 km s^{-1}), we think that it is clear that a higher reference velocity does a better job of fitting the overall spectrum. Nevertheless, this reference velocity is lower than in our published fit to the April 13 spectrum (v_0 = 11,000 km s^{-1}) and does lead to a smaller distance estimate. These differences give an estimate of the errors inherent in the expanding photosphere method, as it is applied by us, and indeed that is how we derive the formal errors that we quote.

6. CONCLUSIONS

We have presented results from a series of model calculations in order to fit the UV and optical spectrum of SN 1993J obtained on 1993 April 15. We require both a high helium composition as well as a significant amount of nonthermal ionization produced by the decay ^{56}Ni → ^{56}Co → ^{56}Fe. We fail to fit the total flux in the UV, finding a value that is consistently low by a factor of 5–10. This may be due to our LTE treatment of Fe II or to failure to correctly model the incident radiation from circumstellar material. Simple models of this

radiation produce no observable effects on the UV and optical region of the spectrum.

We thank David Jeffery, Lisa Ensman, Alex Filippenko, Brian Schmidt, Giora Shaviv, Sumner Starrfield, and Rainer Wehrse for helpful discussions, David Jeffery and Alex Filippenko for providing spectra electronically in advance of publication, and the referee for helpful comments. This work was supported in part by NASA grant NAGW-2999, a NASA LTSA grant to ASU, NASA grant GO-2563.01-87A from the Space Telescope Science Institute, which is operated by the Association of Universities for Research in Astronomy, Inc., and by NSF grant AST 91-15061. Some of the calculations in this paper were performed at the NERSC, supported by the US DOE, and we thank them for a generous allocation of computer time.

REFERENCES

Baron, E., & Hauschildt, P. H. 1993, in preparation
Baron, E., Hauschildt, P. H., Branch, D., Wagner, R. M., Austin, S. J., Filippenko, A. V., & Matheson, T. 1993, ApJ, 416, L21
Bartunov, O. S., Blinnikov, S. I., Pavlyuk, N. N., & Tsvetkov, D. 1994, A&A, in press
Baschek, B., Scholz, M., & Wehrse, R. 1991, A&A, 299, 374
Best, M., & Wehrse, R. 1993, A&A, in press
Brent, R. P. 1973, Algorithms for Minimization without Derivatives (Englewood Cliffs: Prentice Hall)
Filippenko, A. V., & Matheson, T. 1993, IAU Circ. 5787
Filippenko, A. V., Matheson, T., & Ho, L. C. 1993, ApJ, 415, L103
Freedman, W. L., et al. 1993, preprint
Garvey, R. H., & Green, A. E. S. 1976, Phys. Rev. A, 14, 946
Hauschildt, P. H. 1992a, J. Quant. Spectrosc. Rad. Transf., 47, 433
———. 1992b, ApJ, 398, 224
———. 1993, J. Quant. Spectrosc. Rad. Transf., 50, 301
Hauschildt, P. H., Best, M., & Wehrse, R. 1991, A&A, 247, L21
Hauschildt, P. H., Starrfield, S., Austin, S., Wagner, R. M., Shore, S. N., & Sonneborn, G. 1994, ApJ, in press
Hauschildt, P. H., Wehrse, R., Starrfield, S., & Shaviv, G. 1992, ApJ, 393, 307
Höflich, P., Langer, N., & Duschinger, M. 1993, A&A, 275, L29
Hu, J. Y., Li, Z. W., Jiang, X. J., & Wang, L. F. 1993, IAU Circ. 5777
Jeffery, D. J., et al. 1993, ApJ, 421, L27
Kurucz, R. 1993, CD-ROM No. 1, Atomic Data for Opacity Calculations, unpublished
Lotz, W. 1967a, ApJS, 14, 207
———. 1967b, Journal Opt. Soc. America, 57, 873
———. 1968a, Journal Opt. Soc. America, 58, 236
———. 1968b, Journal Opt. Soc. America, 58, 915
———. 1968c, Z. Physik, 216, 241
Meyerott, R. E. 1980, ApJ, 239, 257
Nomoto, K., Suzuki, T., Shigeyama, T., Kumagai, S., Yamaoka, H., & Saio, H. 1993, Nature, 364, 507
Podsiadlowski, P., Hsu, J. J. L., Joss, P. C., & Ross, R. R. 1993, Nature, 364, 509
Rybicki, G. B., & Hummer, D. G. 1991, A&A, 245, 171
Schmidt, B. P., et al. 1993, Nature, 364, 600
Shigeyama, T., Suzuki, T., Kumagai, S., Nomoto, K., Saio, H., & Yamaoka, H. 1994, ApJ, in press
Swartz, D. 1991, ApJ, 373, 604
Swartz, D. A., Clocchiatti, A., Benjamin, R., Lester, D. F., & Wheeler, J. C. 1993, Nature, 365, 232
Tanaka, Y. 1993, IAU Circ. 5753
Wheeler, J. C., & Filippenko, A. V. 1994, in Supernovae and Supernova Remnants, ed. R. McCray & Z. W. Li (Cambridge: Cambridge Univ. Press), in press
Woosley, S. E., Eastman, R., & Weaver, T. A. 1993a, ApJ, in press
Woosley, S. E., Eastman, R., Weaver, T. A., & Pinto, P. 1993b, ApJ, in press
Woosley, S. E., Pinto, P., Ensman, L. 1988, ApJ, 324, 466